Title

Abnormal early cleavage events predict early embryo demise: sperm oxidative stress and early abnormal cleavage.

Journal

Scientific reports, 4(1)

ISSN

2045-2322

Authors

Burruel, Victoria

Klooster, Katie

Barker, Christopher M

et al.

Publication Date

2014-10-01

DOI

10.1038/srep06598

SCIENTIFIC REPORTS

OPEN

SUBJECT AREAS:
EXPERIMENTAL MODELS OF DISEASE
EMBRYOLOGY

Received
14 April 2014

Accepted
18 September 2014

Published
13 October 2014

Correspondence and requests for materials should be addressed to S.M. (smeyers@ucdavis.edu)

Abnormal Early Cleavage Events Predict Early Embryo Demise: Sperm Oxidative Stress and Early Abnormal Cleavage

Victoria Burruel[1], Katie Klooster[1], Christopher M. Barker[2], Renee Reijo Pera[3] & Stuart Meyers[1]

[1]Department of Anatomy, Physiology and Cell Biology, School of Veterinary Medicine, University of California, Davis, [2]Department of Pathology, Microbiology, and Immunology, School of Veterinary Medicine, University of California, Davis, [3]Department of Obstetrics and Gynecology, School of Medicine, Stanford University.

Human embryos resulting from abnormal early cleavage can result in aneuploidy and failure to develop normally to the blastocyst stage. The nature of paternal influence on early embryo development has not been directly demonstrated although many studies have suggested effects from spermatozoal chromatin packaging, DNA damage, centriolar and mitotic spindle integrity, and plasma membrane integrity. The goal of this study was to determine whether early developmental events were affected by oxidative damage to the fertilizing sperm. Survival analysis was used to compare patterns of blastocyst formation based on P2 duration. Kaplan-Meier survival curves demonstrate that relatively few embryos with short (<1 hr) P2 times reached blastocysts, and the two curves diverged beginning on day 4, with nearly all of the embryos with longer P2 times reaching blastocysts by day 6 ($p < .01$). We determined that duration of the 2nd to 3rd mitoses were sensitive periods in the presence of spermatozoal oxidative stress. Embryos that displayed either too long or too short cytokineses demonstrated an increased failure to reach blastocyst stage and therefore survive for further development. Although paternal-derived gene expression occurs later in development, this study suggests a specific role in early mitosis that is highly influenced by paternal factors.

Blastocyst formation in vitro is used as an endpoint in human and animal models to signify developmental competence. This outcome is used clinically in Assisted Reproductive Technology (ART) programs. However, 50–70% of human embryos reportedly fail to develop to blastocysts and this is similar for some animal models[1,2]. Recent studies have revealed that early cleavage events in the embryo had a significant role in determining the developmental fate of the embryo including blastocyst formation and ploidy[3–5].

Non-invasive time-lapse embryo imaging has provided insight into abnormal cleavage errors previously known to occur, but difficult to detect, without constant visualization of the developing embryos inside the incubator[3,5–8]. Preimplantation genetic screening (PGS) has revealed that embryos with abnormal cleavage errors can develop to blastocysts with chromosomal abnormalities and appear morphologically indistinguishable from normal embryos[3,9–13].

Chromosomal abnormalities in embryos are correlated with decreased implantation, decreased pregnancy rates and spontaneous abortion. While there is a negative selection in humans against development of chromosomally abnormal embryos developing beyond the eight cell stage[12] and/or cavitating morulae, a significant number of chromosomally abnormal blastocysts still develop and may be morphologically indistinguishable from normal (euploid) blastocysts[14]. Most of these chromosomally abnormal blastocysts ultimately result in negative pregnancy outcomes. One potential cause of embryonic failure or demise may be that of paternal influence and using the rhesus macaque model, we have determined that sperm quality has an influence on subsequent embryo development. Our laboratory has demonstrated that embryos produced by ICSI from sperm exposed to high levels of reactive oxygen species (ROS) do not develop beyond the four-cell stage[15]. We hypothesized that embryos produced by ICSI of ROS-treated sperm have early abnormal cleavage events that cannot be visualized within daily periodic observations. These embryos are characterized by micronuclei, DNA fragmentation, asymmetrical blastomeres and arrest before the eight-cell stage; characteristics associated with early cleavage errors and aneuploidy in human embryos[3,7,8].

Our objective in this study was to determine whether early developmental events were predictive for blastocyst development in rhesus macaque embryos since early cleavage kinetics have not been determined in this relevant model for human and animal development. An understanding of prolonged or otherwise abnormal cytokinesis is

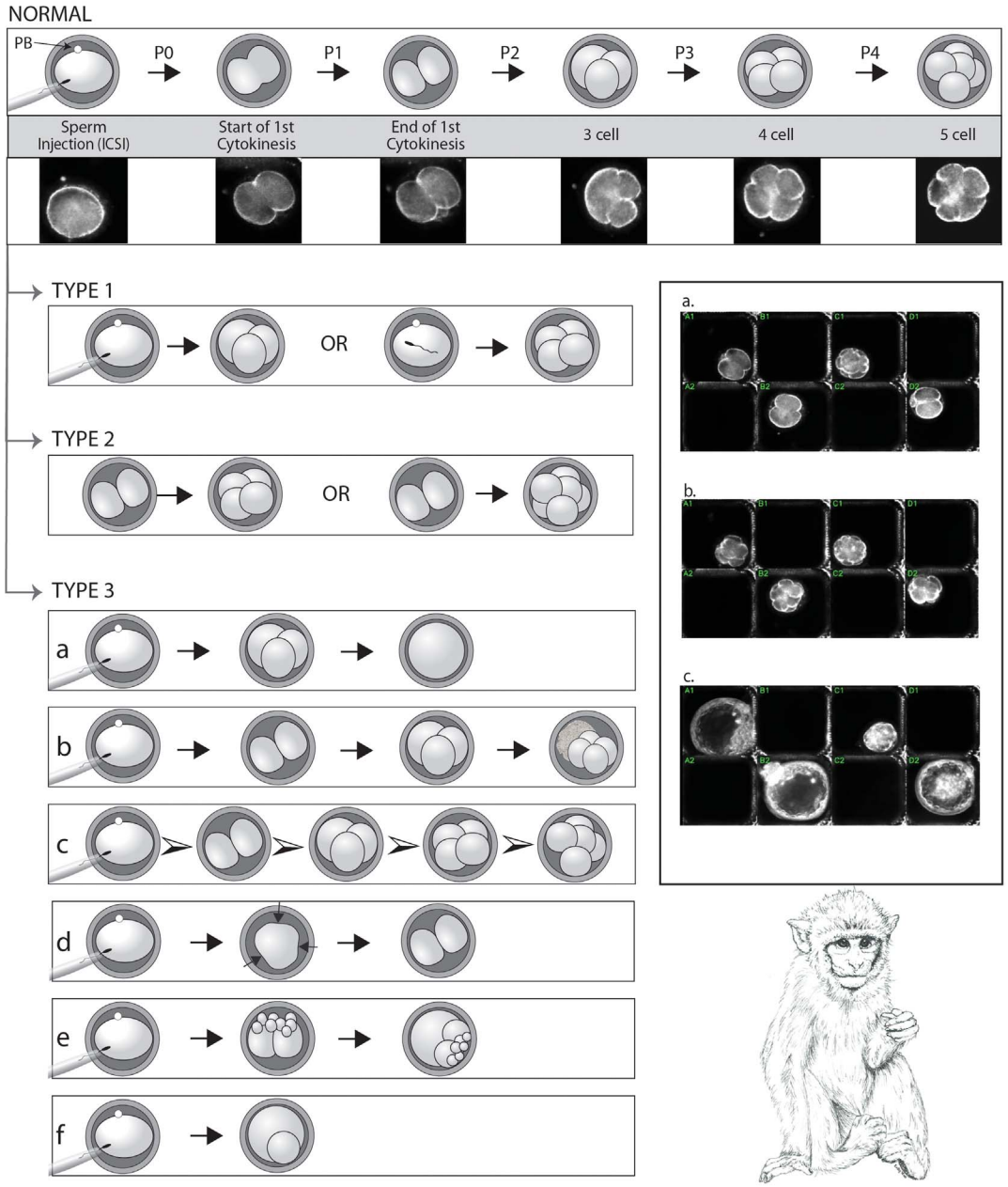

Figure 1 | Rhesus embryo developmental landmarks for duration of cytokinesis in the first five mitotic divisions after fertilization by intracytoplasmic sperm injection (ICSI) and illustration of normal rhesus embryo kinetics including mitotic error types. Inset: images captured from non-invasive time-lapse imaging video showing (a) 2-cell rhesus embryos, (b) 4 to 5-cell rhesus embryos, and (c) expanded blastocysts. Illustration by Kathy West, California National Primate Research Center, © 2014.

an essential first step in determining the influence of extrinsic factors on fetal loss, spontaneous abortion, birth defects, gamete aging, and environmental toxicant exposure. We used a noninvasive time-lapse imaging system to observe the possible early cleavage abnormalities in the first through fourth mitotic divisions of normal embryos and those fertilized by ROS-treated sperm. Survival analysis was used to assess cytokinetic events during early rhesus development for predictive outcomes assessment.

Methods

Reagents/chemicals. The fluorochromes C_{11}-BODIPY (4,4-difluro-5-(4-phenyl-1,3-butadienyl)-4-bora-3a,4a-diaza-s-indacene-3-undecanoic acid) and propidium iodide (PI) were obtained from Invitrogen (Eugene, OR). All other chemicals were obtained from Sigma Chemical Co. (St. Louis, MO) unless otherwise stated.

Animals and sperm preparation. Animals were housed at California National Primate Research Center and maintained according to Institutional Animal Care and Use Committee (IACUC) protocols at the University of California. All experimental methods were approved by the University of California IACUC in accordance with American Veterinary Medical Association and United States Department of Agriculture USDA Guidelines.

Semen samples were obtained by electroejaculation from 2 male rhesus macaques (*Macaca mulatta*) as previously described[16]. Semen samples were collected directly into 50 ml centrifuge tubes containing 5 mL of HEPES-Biggers, Whitten, and Whittingham (BWW) media. Following semen collection, the coagulum was removed and samples were centrifuged for 8 minutes. The pellet was diluted in 5 ml HEPES-BWW containing 1 mg/ml polyvinylalcohol (PVA) and total and progressive motility were determined. Two and a half milliliters of diluted semen were layered over 3 mL of 80% buffered Percoll® and centrifuged at 300 × g for 25 minutes as previously described[17,18]. Following centrifugation, the supernatant was removed; the pellet washed twice in HEPES-BWW with 1 mg/ml PVA (300 × g, 5 minutes); and spermatozoa were resuspended in BWW with 1 mg/ml PVA to a final concentration of 25 × 10^6/ml in 500 µl aliquots. Sperm motility and viability were determined in all

ejaculates prior to each experiment using previously reported methods[15,19]. Sperm total and progressive motility was evaluated by means of computer-assisted sperm analysis (CASA) with HTM Ceros, version 14 (Hamilton Thorne Biosciences, Inc, Beverly, MA). Since ROS-treated sperm lost significant motility after treatment, we also analyzed post-treatment motility using manual motility and forward progression assessment according to parameters for human sperm established by the World Health Organization[20]. A 10 μl drop of sperm suspension was placed on a slide and a coverslip placed over it. At least 200 sperm were counted per slide and triplicate aliquots were counted for total and forward progression. Spermatozoa were diluted to 1×10^6 sperm/ml and analyzed by flow cytometry. The viability probe propidium iodide (PI, final concentration 12 μM) was added during the last 5 minutes of control and treatment incubations so that nonviable lipid-peroxidized cells could be distinguished from live lipid-peroxidized cells using the flow cytometer (data not shown). Viability was determined by the percentage of PI negative cells. Flow cytometry was performed using a FACScan flow cytometer (Becton-Dickenson, Franklin Lakes, NJ, USA) equipped with a 488 nm excitation laser and data was analyzed using CellQuest software (Becton-Dickenson). The fluorescence lipid probe C_{11}-BODIPY (4,4-difluro-5-(4-phenyl-1,3-butadienyl)-4-bora-3a,4a-diaza-s-indacene-3-undecanoic acid) was used to confirm lipid peroxidation levels in induced oxidative stress treatment as previously reported[15,19]. Sperm that were selected for ICSI were not subjected to C_{11}-BODIPY fluorescence staining.

Induction of reactive oxygen species (ROS) in sperm. A xanthine-xanthine oxidase (XXO) ROS-producing system was used to induce ROS production in rhesus monkey sperm as previously reported[15,19,21,22]. The XXO system primarily results in generation of superoxide anion and hydrogen peroxide. Sperm at a concentration of 25×10^6/ml were incubated for 135 minutes (T_{135}) with or without 1 mM xanthine and 1 mM xanthine oxidase at 37°C, 5%CO_2 in air. Sperm motility was evaluated at 0 (T_0) and 135 minutes (T_{135}), and the samples were processed for determination of viability and lipid peroxidation. The lipid peroxidase promoters, ferrous sulfate (1 μM) and sodium ascorbate (5 μM) were added to both treatments. Sperm were washed in BWW and centrifuged for 3 minutes at 300 × g. Sperm selected for ICSI were further diluted with BWW containing 1 mg/ml PVA to a final sperm concentration of 4×10^6/ml.

Superovulation, oocyte collection, and intracytoplasmic sperm injection (ICSI). Females scheduled for necropsy for non-reproductive reasons, with a history of regular menstrual cycles, were selected as oocyte donors for superovulation and oocyte collection. Beginning on days 1–4 of menses, females were superovulated with injections of recombinant human follicle stimulation hormone (rhFSH, 30 I.U., intramuscular (i.m.), twice daily, Follistim®, Merck, Whitehouse Station, NJ) for 6 consecutive days. On day 7, a single injection of the gonadotropin releasing hormone antagonist Acyline (75 μg/kg/bw, subcutaneous) was administered. Injections of purified urinary human luteinizing hormone and human follicle stimulation hormone (hLH, 30 I.U., and hFSH, 30 I.U.) were administered as subcutaneous injections twice daily (Menopur, Ferring Pharmaceuticals, Parsippany, NJ) days 7–8 of superovulation treatment. A single injection of human chorionic gonadotropin (1300 I.U., i.m., Ovidrel®, EMD Serono, USA) was given 35 hours before follicular aspiration. At necropsy, follicles of the excised ovaries were punctured using a sterile 1.5-inch, 20-gauge needle attached to mild vacuum pressure into 15 ml sterile tissue culture tubes of Tyrode's albumin lactate pyruvate medium buffered with HEPES (TALP-HEPES) at 37°C and immediately transported to the laboratory for recovery of oocytes at 37°C. Only progressively motile sperm were individually selected for embryo production for control sperm. Embryos were produced using ICSI of mature metaphase II (MII) oocytes as described previously using XXO-treated sperm and control sperm[23–25]. Only visibly motile sperm observed as having at least moderately beating tails were chosen for injection for the XXO treated sperm. Injected oocytes were cultured in 25 μl drops of Global® embryo culture medium (LifeGlobal, Guilford, CT) supplemented with 10% serum protein supplement under oil (Ovoil®, VitroLife, USA) and cultured at 37°C in a humidified incubator containing 6%CO_2, 5%O_2 and 89%N_2.

Embryo evaluation. Embryos were assessed at 16 hours post-ICSI for the presence of two pronuclei (PN) and transferred to specialized 25-well dishes (Auxogyn, Menlo Park, CA) that allow group culture of 25 embryos in a single drop of 30 μL of medium with a 2 mL overlay of oil. Embryos were cultured for six days at 6% CO_2, 5% O_2 and 89%N_2 in Global® medium supplemented with 10% serum protein supplement (LifeGlobal) from day 1 to day 3 and in Global® medium supplemented with 10% fetal bovine serum (Invitrogen, Carlsbad, CA) from day 3 to day 6.5. Upon completion of time-lapse imaging at day 6.5, all embryos were evaluated for cell number and blastocyst development and photographed on a phase contrast microscope. Blastocysts were categorized into early blastocyst, full blastocyst, expanded blastocyst, and hatching blastocyst in accordance with Gardner's grading system[26–28].

Noninvasive time-lapse imaging. Imaging was performed with a time-lapse enabled high-resolution, dark-field imaging system that includes specialized microscopes that fit into an incubator such that embryos develop without removing them from the incubator for media changes[3–5,7]. This allows group culture of embryos within a single droplet of medium, image capture every 5 minutes with conversion to AVI movies, and analysis of key cell division time marks (Early Embryo Viability Assessment [*Eeva*™] (Auxogyn, Menlo Park, CA). Each embryo was analyzed for four mitotic parameters that have been described in detail[3,4,7] and shown schematically in Figure 1:

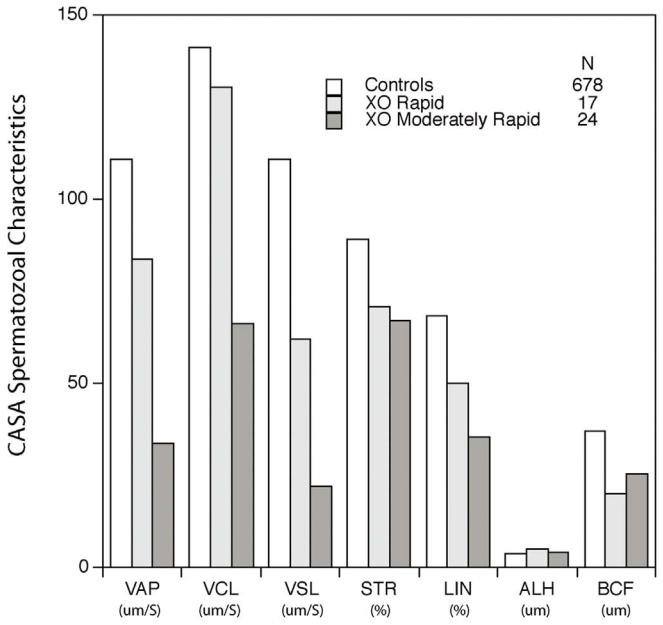

Figure 2 | Measurement of spermatozoal motility for control and XXO-treated sperm selected for ICSI using computerized sperm analysis (CASA). Levels of significance are not shown due to small sample sizes for manually selected tracks for XXO sperm. VAP = average path velocity, VCL = curvilinear velocity, VSL = straight line velocity, STR = straightness, LIN = linearity, ALH = lateral head amplitude, BCF = beat cross frequency.

P0, the duration from the time of ICSI to the start of 1st cytokinesis; P1, duration of the first cytokinesis that results in two daughter cells; P2, the time interval between the first mitosis and start of the second mitosis; P3, synchronicity of the second and third mitosis; and P4, time between third and fourth mitosis that results in two sets of granddaughter cells. Data were recorded in a Microsoft Excel spreadsheet with macros for conversion of time-stamped sequential images into minutes and hours of incubation with each video frame represented at five minute intervals.

Abnormal cleavage assessment. Normal cleavage parameters are schematically defined in Figure 1. During the first cytokinesis the embryo divides into two distinct blastomeres of equal size. One of these blastomeres initially divides giving rise briefly to three blastomeres and the third blastomere divides by mitotic division resulting in a total of four blastomeres. As these divisions are not synchronous in most mammals, there are transiently odd numbers of blastomeres. Abnormal cleavage patterns observed in this study were organized into 3 types as illustrated in Figure 1: Type 1) the first mitosis resulting in three or more blastomeres at the first cytokinesis, Type 2) embryos that divided from a two-cell embryo directly into 4- or more blastomeres[29]. Type 3 embryos that had one or a combination of the following abnormalities: a) embryos that reabsorbed blastomeres before mitotic cleavages 3 and 4; b) after the 2-cell stage, one of the blastomeres does not undergo mitosis and only one of the original two blastomeres contributes to the embryo participating in all subsequent cleavages; c) extremely fast dividing embryos (depicted by arrowheads); panel d) embryos that had multiple cleavage sites at first observation or then delayed the start of cytokinesis and subsequently divided into two cells; e) embryos with 10–25% fragments at 1st cleavage; and f) embryos that were very asymmetrical at 1st cleavage.

Embryo staining and fluorescence imaging. Embryos were fixed in a 2% paraformaldehyde PIPES buffer with 0.5% Triton X-100 and incubated for 30 minutes at 37°C. The embryos were washed twice in 0.5 ml of blocking solution (PBS with 5% BSA, 0.5% FBS, 62.4 μM glycine, and 0.01% Triton X-100) and transferred to 0.5 ml of blocking solution and incubated for 1 hour. Embryos were then incubated individually in 10 μl drops with monoclonal anti-α-tubulin-FITC antibody produced in mouse (Sigma, St. Louis, MO) diluted in DPBS (1 : 100), with 0.3 mls of mineral oil covering the drops at 37°C for 1 hour. After 2 washes in 0.5 ml blocking solution they were incubated for 10 minutes in 0.4 ml of 10 μM of Hoescht 3342. After staining, embryos were individually mounted into 13 μl of Prolong® Gold antifade reagent (Invitrogen, Grand Island, NY) on a slide, a coverslip was gently placed to cover the embryo, and this was allowed to harden overnight at room temperature before they were imaged. Images for confocal microscopy were acquired using a 40×/NA 1.0 lens on an Olympus FV1000 Spectral Scan point scanning confocal running Olympus FluoView version 2.1 software (Olympus, Inc., USA). Laser excitation lines and detector slits were set appropriately for Alexa488 and DAPI channels (488 and 358 nm excitation). Noise in individual optical sections was reduced by summing

Table 1 | Distribution of cleavage patterns in rhesus macaque embryos

Group	No. of embryos	Total Normal (%)	Total Abnormal (%)	Abnormal Types		
				Type 1 (%)	Type 2 (%)	Type 3 (%)
Blastocysts	30	24 (80)	6 (20)	3 (10)	2 (6.7)	1 (3.3)
Non-blastocyst	29	6 (20)	23 (79)	13 (45)	3(10)	7(24)

multiple scans of each image ("Kalman filtering"). Differential Interference Contrast (DIC) images were recorded using unabsorbed excitation light at 488 nm. Three dimensional images were recorded after acquiring z-stack images of 1.62 um per sequential focal slice. Image visualization and analysis employed Olympus FluoView software (Olympus, Inc., USA).

Statistics. Survival analysis was performed using the survival package in R version 3.0 (R Core Team 2013). Specifically, separate Kaplan-Meier survival curves were fitted for embryos based on whether there was an unusually brief period of <1 hour between the 2-cell and 3-cell divisions ("abnormal") or a more typical interdivision period of >1 hour ("normal"). The survival curves were compared using a Mantel-Haenszel test with a threshold of $p < 0.05$ for significance. The percentages of embryos that resulted in viable blastocysts were compared after grouping by the length of the interdivision period by exact binomial tests. Comparisons for P0, P1, P2, P3 and P4 data were done using Student's T-test (JMP software, SAS Institute Inc., Cary, NC). Differences were considered significant when p-values were < 0.05.

Results

Characteristics of rhesus macaque sperm used for ICSI. Sperm processed for ICSI were analyzed using motility and viability endpoints. For sperm used to establish embryo developmental parameters, viability/membrane integrity of ICSI-selected sperm was not different between sperm samples and was 95 +/− 2% for control and 90 +/− 5% for XXO treatments. Motility, as expected, was decreased ($p > 0.01$) in XXO treated sperm used for ICSI in comparison to that of control sperm used for ICSI. Control sperm used for ICSI were subjectively selected from the most rapidly moving sperm that were progressively motile while XXO-treated sperm were selected for ICSI if they displayed progressive motility and at least rapid or moderately rapid motility resulting from XXO treatment. Figure 2 demonstrates motility characteristics compared among control sperm and XXO treated sperm.

Characteristics of normal embryos reaching blastocyst stage. Early embryo cleavage was analyzed retrospectively by converting sequential time-lapse images to avi movies to record the cleavage pattern and timing of mitotic divisions of embryos that resulted in blastocysts. We used these data to predict blastocyst formation in very early embryos using the parameters P0–P4. Normal cleavage was defined as cleavage of a zygote to a two-celled embryo followed by the cleavage of one blastomere at a time up to the five-cell stage. Any deviation from this normal cleavage would be considered an abnormal cleavage pattern as described above. Of 77 MII oocytes injected with control sperm, 67 oocytes were fertilized (87.0%) based on visualizing two pronuclei (Table 1). Eight embryos were excluded from cleavage assessment: two embryos had cleaved before starting the video, four were excluded due to inadequate visualization assessment of cleavage and two failed to cleave. Of the remaining 59 embryos assessed, 30 (50.9%) reached blastocyst and 29 (49.1%) embryos arrested and failed to reach blastocyst by day 6.5. Cleavage patterns were assessed for the 59 embryos and parameters P0–P4 calculated for each embryo. Embryos were then retrospectively divided into two groups (Table 2): those that reached the blastocyst stage by day 6.5 (blastocysts) and those that did not reach this stage by day 6.5 (non-blastocysts).

Embryos reaching blastocyst stage by day 6.5 (n = 30) consisted of nine (30%) early blastocysts, three (10%) full blastocysts, thirteen (43.3%) expanded blastocysts, and five (16.7%) hatching blastocysts (Figure 3). In this group, 80% of the embryos exhibited a normal cleavage pattern and timing of mitoses and 20% of the embryos exhibited an abnormal cleavage pattern (Figure 4). The abnormal cleavage observed in embryos reaching blastocyst stage were 10% (3/30) of the embryos with Type 1 cleavage pattern, 6.7% (2/30) displayed Type 2 cleavage pattern; and 3.3% (1/30) displayed Type 3 cleavage pattern (Table 1). These blastocysts were characterized by low total cell number indicated by small size, excluded cells, absence of an ICM in a few instances, disorganized ICM formation, and large cells visible inside the blastocoels (figure 5).

Survival analysis was used to compare patterns of blastocyst formation based on P2 duration. Kaplan-Meier survival curves (Figure 6) demonstrate that relatively few embryos with short (<1 hr) P2 times reached blastocysts, and the two curves diverged beginning on day 4, with nearly all of the embryos with longer P2 times reaching blastocysts by day 6 (Mantel-Haenszel $p = 0.003$). Embryos not reaching blastocyst stage are shown as a higher percentage since the data are described as percentage of embryos *failing* to reach blastocyst stage. These data demonstrated that success in reaching the blastocyst stage could be predicted by early P2 durations estimated using time-lapse analysis.

The majority (62%) of the non-blastocyst embryos arrested before reaching the morula stage and the remaining embryos (38%) arrested at the morula stage. In those embryos not reaching blastocyst stage (n = 29), two embryos (6.9%) arrested at the 6-cell stage (<8-cell); two embryos (6.9%) arrested at the 8-cell stage without compaction (8-cell); thirteen embryos (44.8%) arrested before reaching morula without compaction (>8-cells); and twelve embryos (41.4%) developed into morulae. For nonblastocysts, 69% of the embryos exhibited an abnormal cleavage pattern and 31% of the embryos exhibited the normal cleavage pattern. The distribution of abnormal cleavage patterns for nonblastocysts were: 45% (13/29) embryos in the had Type 1 cleavage; 10% (3/29) embryos displayed Type 2 cleavage; 24% (7/29) displayed Type 3 cleavage; and 20% (6/29) had a normal cleavage pattern during the observed time (Table 1).

Table 2 | Early cleavage parameters for embryos that reached early blastocyst by day 6.5 and embryos that did not become blastocysts by day 6.5

	P0 (h)	P1 (h)	P2 (h)	P3 (h)	P4 (h)
Blastocyst	22.5 ± 0.3	0.2 ± 0.04	7.6 ± 0.8	2.5 ± 0.6	7.3 ± 0.8
n	30	30	30	30	30
Non-blastocyst	22.3 ± 0.4	0.8 ± 0.4	4.5 ± 0.8*	2.8 ± 0.7	7.4 ± 1.4
n	29	29	29	27	27

Data expressed as mean ± standard error of the mean (SEM).
*Significant difference between treatment groups ($p < 0.05$). –t-test.

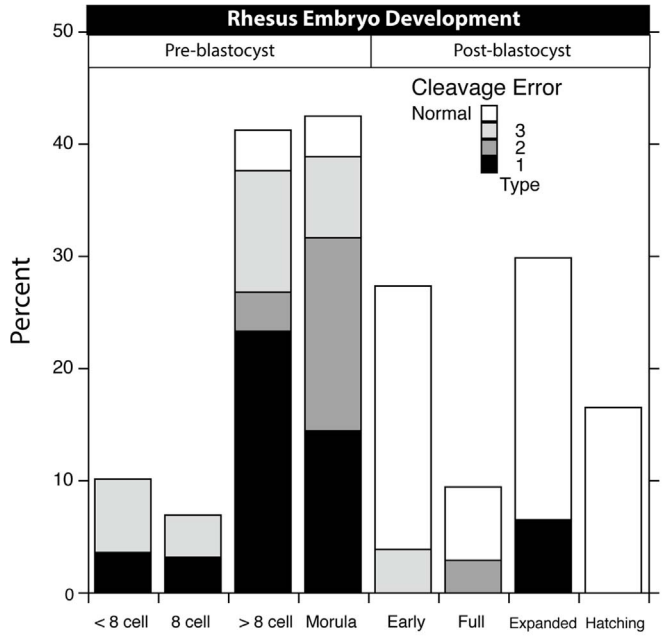

Figure 3 | Rhesus embryo development demonstrating prevalence of cleavage errors by type in pre-blastocyst and post-blastocyst development.

Mitotic characteristics of early rhesus macaque embryos. We compared the early cleavage parameters, P0, P1, P2, P3 and P4 in order to determine whether predictive values for blastocyst development could be assessed. The values for parameters, P0, P1, P2, P3 and P4 for blastocysts or nonblastocysts are presented in Table 3. The length of time between the end of the first cytokinesis and the start of the cleavage to a 3-cell embryo (P2) was found to be significantly different between blastocysts (7.6 ± 0.8) and non-blastocysts (4.5 ± 0.8 hours $p = 0.007$). Parameters P0, P1, P3 and P4 were not found to be different between embryos reaching blastocyst stage and those that did not reach blastocyst ($p > 0.10$). The majority of embryos that reached the blastocyst stage had P2 durations greater than one hour. Type 1 cleavage pattern was the most prominent abnormal pattern in the embryos not reaching blastocyst stage. This pattern resulted in a P2 calculation of zero since these embryos did not undergo a 2-cell to 3-cell division. Some abnormal embryos (Type 3) also undergo very fast cleavage that results in P2 of less than one hour. To further analyze this trend, we analyzed embryos and stratified them according to two categories: those with a P2 greater than one hour ($n = 43$) and those with P2 less than one hour ($n = 16$) (Table 3). The average P2 duration was 8.7 h ± 2.8 for the former and 0.06 h ± 0.2 for the latter embryo groups. For 43 embryos taking longer than one hour to complete P2, 26 (61%) reached blastocyst and 17 (39%) embryos were arrested prior to the blastocyst stage. In contrast, four embryos (25%) developed into blastocysts when P2 was less than one hour and twelve (75%) embryos were arrested prior to blastocyst stage. In summary, if P2 was less than one hour, fewer blastocysts were produced than when P2 was greater than one hour in duration ($p = 0.048$). Next, to evaluate the relationship between abnormal cleavage and P2 less than one hour, embryos were categorized as: 1) arrested embryos and blastocysts with abnormal cleavage patterns, or 2) blastocysts resulting from the normal cleavage pattern. Of the embryos with a P2 duration greater than one hour, twenty-three (54%) embryos had normal cleavage patterns and all were blastocysts (Figure 5) whereas twenty (46%) embryos had abnormal cleavage and were arrested. Of the embryos with P2 durations of less than one hour, fifteen (94%) embryos had an abnormal cleavage pattern, five were blastocysts and one (6%) embryo had a normal cleavage pattern and was a blastocyst. Embryos with P2 greater than one hour had the potential to reach blastocyst although only five embryos reached this stage (Figure 6).

Since the 'successful' blastocyst category was comprised of embryos ranging from early to hatching blastocyst by day 6.5, it is apparent that the blastocysts were cleaving at different rates. To further understand this observation, analysis of developmental intervals were examined. The blastocysts were divided into two subcategories: embryos that reached early or full blastocyst by day 6.5 ($n = 12$); and embryos that reached expanded or hatching blastocysts by day 6.5 ($n = 18$). The durations of P0–P4 were compared for the two subcategories (Table 4). The following intervals (Table 5) were also compared: the start of first cleavage (P1) to the 4-cell (P3) stage, 4-cell to 8-cell stage, the 5-cell (P4) to 8-cell stages, the 8-cell stage to the start of compaction, the 8-cell stage to the start of cavitation, the durations from P1 to start of compaction, and P1 to the early blastocyst stage.

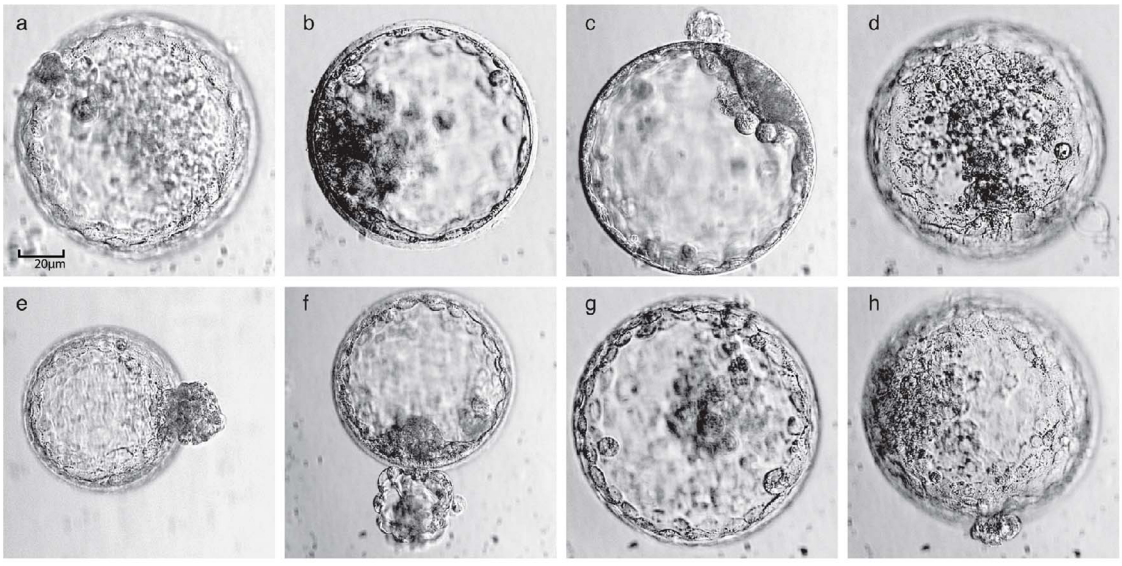

Figure 4 | Examples (a–h) of rhesus blastocysts recovered at day 6.5 that developed from normal cleavage patterns but with duration of the second cytokinesis (P2) greater than one hour. Bar = 20µ.

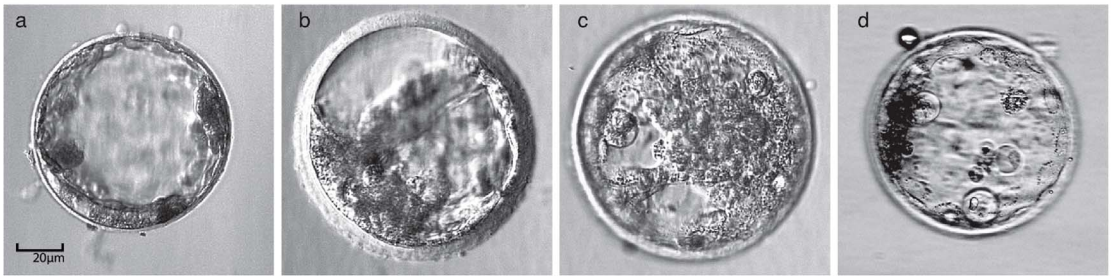

Figure 5 | Examples of rhesus blastocysts recovered at Day 6.5 resulting from abnormal cleavage patterns but with duration of the second cytokinesis (P2) less than one hour. The latter is typical for normal embryos. This figure demonstrates a small number of embryos that demonstrated normal timings of cytokinesis but had early abnormal cleavages at 2–4 cell stage. Bar = 20µ.

A slow developmental trend was evident for early or full blastocyst embryos throughout most of the durations analyzed from P1 to early blastocyst stage when compared to expanded and hatched embryos (Table 5), but the individual parameters P0–P4 did not show a significant difference between the two groups (Table 4). The duration from a 5-cell embryo to an 8-cell embryo was the most significantly different interval observed between the two groups, 27.0 h ± 3.5 (SE) for the former and 14.8 h ± 2.6 (SE) for the latter ($p = 0.008$). Also significant were the following durations: time of the first cleavage to the 4-cell stage; 4-cell to 8-cell; compaction to cavitation; P1 to compaction and P1 to early blastocyst. However the comparison of the durations 8-cell stage to compaction and 8-cell to cavitation were not significantly different.

Our data demonstrate that, in addition to variation in P2 duration, successful blastocysts demonstrated slower cleavage during the 5-cell stage to the 8-cell stage. This interval is the time in which rhesus embryos are undergoing embryonic genomic activation (EGA) during the progression from 6–8 cells. These data also demonstrate that embryos that reached expanded and hatching blastocyst by day 6.5 cleaved faster at most intervals analyzed than non-expanded blastocyst.

Oxidative stress in sperm results in abnormal cleavage and failure of blastocyst formation in rhesus zygotes. Since all the embryos produced in the experiment discussed above were produced from untreated sperm and oocytes, all the data for the parameters P0 through P4 were combined as a control group to compare developmental differences in embryos resulting from oxidatively stressed sperm. Previous studies in our laboratory demonstrated that embryos resulting from fertilization using XXO-treated sperm never developed to blastocyst and usually arrest before post-fertilization day 3 at what appeared to be the 4–6 cell stage[15]. We hypothesize that these embryos have early defective cleavage events that include abnormal cleavage patterns and delayed cleavage compared to control embryos. Our objective was to determine the stage at which these embryos might be most vulnerable to mitotic errors. Twenty-one MII oocytes from three different egg donors were injected with XXO treated sperm resulting in fifteen (71.4%) fertilized embryos. Abnormal cleavage patterns were observed in all XXO embryos in this study. While embryo culture was stopped on day 2.5, some embryos had as many as 6–7 blastomeres visible after only two mitotic divisions. It is apparent from time-lapse imaging that these represent cleavage errors of Types 1–3. Normal cleavage patterns were not seen during cleavage of the XXO embryos evaluated in the study. Type 1 cleavage abnormalities were observed in 61.5% (8/13) of XXO embryos having a P2 duration of less than one hour, 8% (1/13) displayed Type 2 abnormalities; and 30.8% (4/13) displayed Type 3 abnormalities (Table 6). Some of these embryos had 10 to 20% fragmentation however there did not appear to be a pattern in this small cohort of embryos.

Only P0, P1 and P2 parameters could be compared for all XXO embryos since few XXO embryos cleaved beyond the 3rd mitotic division producing very little data for comparison (Table 7). The interval of time from ICSI (P0) to first cleavage was different ($p = 0.018$) between control and XXO embryos (22.5 ± 0.2 hours vs. 26.0 ± 1.5 hours, respectively). The mean for P1 was not different between the two groups ($p > 0.1$). The P2 durations for the XXO group were different from those of control embryos. The P2 period for the controls was 6.1 ± 0.5 hours and the P2 period for XXO was 3.2 ± 1.2 hours, ($p = 0.02$). The significantly shorter P2 period in the XXO group is attributed to the 61.5% incidence of Type 1 abnormal cleavage pattern in which P2 was equal to zero.

No differences were observed between control and XXO treatment embryos for P3, the synchronicity of second and third mitoses. However, a difference between P4 periods was observed between control (7.0 ± 0.8 hours) and XXO embryos (3.2 ± 2.6 hours), ($p = 0.02$). This large variation indicated that the time between the cleavage of the fifth cell in the XXO group is much faster than for normal embryos. This might indicate a loss of synchronous cell division, or simply a breakdown in mitotic organization. Since the XXO embryos typically were observed as arrested by day 3, the

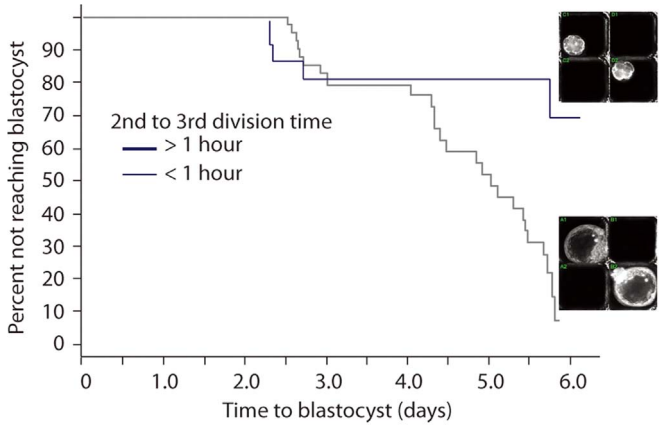

Figure 6 | Kaplan-Meier survival curve of rhesus embryos cultured for up to 6.5 days following ICSI.

Table 3 | Distribution of blastocysts between embryos with P2 duration greater than 1 hr and those embryos with P2 less than 1 hr

	No. embryos	Duration of P2 (hrs)	*No. blastocyst (%)	*No. non-blastocyst (%)
>1 hr	43	**8.7 ± 2.8	26 (60.5%)	17 (39.5%)
<1 hr	16	**0.06 ± 0.2	4 (25%)	12 (75%)

Data expressed as mean ± SEM.
*chi-square test = Fisher's exact test $p = 0.0204$.
**$p = 0.0001$.

Table 4 | Measures of P0 to P4 durations between early to full blastocysts at day 6.5 or embryos that were expanded or hatched by day 6.5

	P0	P1	P2	P3	P4
	(hrs)*	(hrs)	(hrs)	(hrs)	(hrs)
Early-Full Blastocysts (n = 12)	22.4 ± 0.5	0.3 ± 0.1	8.5 ± 1.3	3.8 ± 1.1	6.8 ± 1.4
Expanded-Hatched Blastocysts (n = 18)	22.5 ± 0.4	0.2 ± 0.03	7.0 ± 0.9	1.7 ± 0.5	7.5 ± 1.0
p-value*	0.917/NS	0.32/NS	0.36/NS	0.1/NS	0.67/NS

*Data expressed as mean ± SEM.

culture of the XXO embryos was stopped on day 2.5 and day 4 to examine XXO embryos for cytoskeletal and nuclear abnormalities. Confocal microscopy (Figure 7) of XXO-fertilized rhesus embryos revealed the presence of multiple micronuclei, fragmented nuclei, anucleate blastomeres, and disorganized spindles imaged using DAPI and anti-**α**-tubulin labeling that differed markedly from controls. Chromosomes were not analyzed in this study. In summary, the use of non-invasive imaging parameters showed that the start of first cleavage was delayed in the XXO group and that the majority of embryos in the XX0 group had P2 values of less than one hour due to the Type 1 cleavage pattern. All embryos produced by XXO treated sperm resulted from early cleavage errors. The stained XXO cells also demonstrated that there were nuclear abnormalities associated with these abnormal cleavages as well.

Discussion

Non-invasive imaging of the rhesus macaque embryo. Our data demonstrate that ICSI-produced rhesus embryos complete the first three cell divisions within specific time periods that are related to early blastocyst development by day 6.5. Early events in the first 1–2 days post-fertilization including cytokinesis and mitosis accurately predicted which specific embryos were likely to progress to blastocyst stage. This study suggests that rhesus embryo development closely models that of humans and may serve as an accurate model system to study human development. Although gestation length differs in the two species, early development prior to blastocyst formation appears remarkably similar. Embryos produced from sperm with ROS exposure prior to fertilization exhibit cleavage abnormalities in the 1^{st}–4^{th} mitotic cleavages and a delayed start of 1^{st} cytokinesis compared to control embryos.

Previous studies with human embryos observed that the early cleavage parameters P1, P2 and P3 were predictive of blastocyst formation[5,7] and correlated with euploidy[3]. Embryos outside of optimal ranges of P1, P2, P3 displayed abnormal RNA patterns for cytokinesis, microRNA (miRNA) biogenesis, and maternal mRNA reserves[7]. Chavez and coworkers[3] demonstrated that embryos with sub-optimal P2 durations were associated with mitotic errors, aneuploidy and mosaicism. In our study, embryos with P2 durations greater than one hour were most likely to reach blastocyst by day 6.5. We observed that P2 durations of less than one hour displayed predominantly abnormal cleavage embryos of Types 1 and 3 that were detrimental to embryonic development and subsequently resulted in developmental arrest.

We chose day 6.5 as an endpoint for this study since we[15,25,30] and others[24,31,32] have consistently observed expanded blastocysts at day 6 to day 7 in rhesus embryos. Therefore, an early blastocyst by day 6 was considered normal blastocyst formation for the purposes of this study. We recognize that some embryos in our study could have reached this stage given an additional one-half to one full day of incubation but this would not have changed our assessment of the early cleavage events. This study provides some insight into the cleavage patterns that do result in blastocyst formation in rhesus embryos and to the fate of embryos with abnormal early cleavage patterns.

The temporal development for the blastocysts in this study corresponded to the timelines previously reported for in vivo development previously reported by Goodeaux and coworkers[33]. The rhesus embryo stages were observed in that study after natural mating were as follows: morula by day 4, early blastocysts by day 5 and expanded blastocyst by day 6. However there was a group of embryos that only reached early blastocyst by day 6.5. Slow growth is known to be associated with abnormal blastocyst development in humans and sometimes reflects chromosome abnormalities[3,7,34]. Rhesus aneuploidy was reported in approximately 50% of embryos produced by IVF with an average of 51.3% aneuploid blastomeres per embryo[35]. This rate of aneuploid blastomeres is similar to that found in humans[3,36]. Thus, there is some possibility that the slower growing rhesus embryos could be of sub-optimal quality regardless of the normal early cleavage patterns. While the majority of blastocysts in this study developed from normal cleavage patterns and exhibited normal morphology, we cannot attest to their chromosome status since this was not examined.

Table 5 | Developmental intervals of blastocyst development following ICSI

Embryo stage	Early-full blastocysts n = 12	Expanded-hatched blastocysts n = 18	p-value
1 to 4-cell	12.6 ± 1.6	9.0 ± 0.7	0.03
4 to 8-cell	33.8 ± 3.6	22.4 ± 2.8	0.02
5 to 8-cell	27.0 ± 3.5	14.8 ± 2.6	0.008
8-cell to compaction	41.7 ± 4.8	34.8 ± 4.0	0.29
8-cell to cavitation	60.5 ± 4.6	48.1 ± 4.3	0.06
Compaction to cavitation	18.8 ± 2.6	12.2 ± 1.3	0.02
Compaction to early blastocyst	30.0 ± 2.9	22.1 ± 2.2	0.03
P1 to compaction	88.0 ± 7.4	66.1 ± 4.6	0.02
P1 to early blastocyst	117.9 ± 8.6	88.2 ± 6.1	0.01

Data expressed as mean ± SEM.
$P < 0.01$ represents significant differences within rows.

Table 6 | Percentage of ICSI embryos displaying abnormal cleavage patterns in ICSI embryos fertilized using sperm exposed to xanthine-xanthine oxidase treatment (XXO) in vitro

	Normal	Type 1	Type 2	Type 3
XXO (n = 13)	0.0% (0/13)*	61.5% (8/13)	7.7% (1/13)	30.8% (4/13)

*Mean (%).

The medium used for this study was Global® medium (Life Global) a KSOM^{AA} (potassium simplex optimized medium) based commercial medium available for human embryo in vitro culture[37–39]. A continuous medium was needed for this study because changing media every other day would have disrupted the video recording of this experiment and interfere with the ability to accurately assess the time from start of culture to end of culture. Global® medium with serum protein supplement and FBS from day 3 to day 6.5 produced a group of faster developing embryos than previously observed in our laboratory compared with HECM-9[15] and CMRL and co-culture[25,30] along with a higher percentage of blastocysts.

Abnormal early cleavage errors indicate developmental failure. The majority of successful blastocysts originated from normal early cleavage patterns with only a few originating from abnormal cleavage. The majority of nonblastocyst embryos arrested by day 3 and a few of these embryos progressed to the morula stage and arrested on day 4. The abnormal early cleavage errors observed in this study were similar to those previously reported for human embryos[5–7,9–11]. Although we did not observe oolemmal ruffling and chaotic cleavage as described[40], we have observed these changes in embryos fertilized with oxidatively stressed sperm[15]. The incidence of abnormal cleavage errors during early mitotic events usually resulted in a decreased potential to reach blastocyst stage in this study.

Cellular fragmentation was not widely observed during early cleavages of embryos as is usually seen in humans and could not be used as a separate prognostic factor. Therefore, any evidence of cellular fragmentation was grouped into the Type 3 category, a miscellaneous grouping. Interestingly, fragmentation was observed more commonly in our study after the 8-cell stage in arrested embryos. It was not clear if this fragmentation was associated with cell death, apoptosis, or aneuploidy since embryos were not tested for any of these possibilities. The arrested morulae were morphologically similar to those with 'regional compaction' that have been described in abnormal day 4 morulae[41].

Blastocysts produced from a normal cleavage pattern appeared morphologically normal. However, we understand that morphology alone does not always indicate a normal embryo. Since our embryos were not examined for chromosome abnormalities we cannot attest to the chromosomal makeup of these embryos. A few of the blastocysts produced in this study originated from abnormal early cleavage errors. Previous studies have shown that bovine embryos with direct cleavage to multiple blastomeres can develop into blastocysts with a higher incidence of abnormal morphology and higher incidence of chromosome abnormalities[13,42]. Decreased implantation was observed in abnormal early cleaving human embryos compared to blastocysts originating from normal early cleavage patterns[6]. The morphology of blastocysts in our study produced from Type 1 or Type 2 cleavage were classified as abnormal due to visible low cell numbers in the trophectoderm, lack of ICM, small ICM or visible disorganization of cells within the blastocoel as previously described[13,41]. However, as was also observed in bovine and human studies, one blastocyst in our study formed from a Type 1 abnormal cleavage was morphologically indistinguishable from other blastocysts arising from normal early cleavage.

While all the successful blastocysts had reached a "blastocyst stage" they were obviously developing at different rates. The majority (18) of our blastocysts had expanded by at least day 6.5. The remaining embryos (12) were at early blastocyst and full blastocyst by day 6.5. Previous studies have shown that the use of time-lapse retrospective analysis can reveal specific cleavage intervals at which suboptimal embryos might exhibit slower post-cleavage developmental rates than optimal embryos[6,9–11]. Cleavage intervals were reported to be significantly different in the 4–8 cell and 5–8 cell for expanded versus non-expanded human blastocysts with the expanded embryos cleaving at a faster rate[11]. Another set of studies demonstrated significant longer durations from the 8-cell stage to compaction and the 8-cell stage to cavitation between embryos that were aneuploid in comparison to euploid embryos[9]. Our analysis shows that the most significant stage at which the slower developing rhesus embryos demonstrated a lag in cleavage was at the 5–8 cell duration. Rhesus embryos are known to undergo EGA at the 6–8 cell stage very similarly to human embryos. However, we did not find significant differences in this study for the durations from 8-cell to compaction or 8-cell to cavitation, but we did find significant differences for the interval from compaction to cavitation between the two groups. This could be due to the small size of our sample set.

It is our experience and that of others that some non-human primate embryos will become expanded blastocysts and hatch by day 7–8[23,24,43]. Nevertheless, there are no studies, including this one, that compare the potential of early or late expanding blastocyst embryos in rhesus macaque to embryo quality such as ploidy or ability to implant. However, we do confirm that rhesus embryos exhibit a significantly slower cleavage rate at the 5–8 cell stage and from compaction to cavitation similar to human embryos that are unlikely to reach expanded blastocyst stage in vitro. Also, while our data for blastocyst prediction shows that the potential to reach blastocyst stage could be determined by the P2 parameter, this parameter could not distinguish between a slow and fast group of blastocysts.

Table 7 | Rhesus embryo parameters for embryos fertilized with XXO-treated sperm

	P0 (h)	P1 (h)	P2 (h)	P3 (h)	P4 (h)
Control	22.5 ± 0.2*	0.5 ± 0.2	6.1 ± 0.6*	2.7 ± 0.4*	7.3 ± 0.8
n	59	59	59	58	57
XXO	26.0 ± 1.5*	0.7 ± 0.5	3.2 ± 1.7*	9.1 ± 2.6*	4.8 ± 1.6
n	13	13	13	5	5

Data expressed as mean ± SEM.
*Significant difference between treatment groups ($p < 0.05$) within columns.

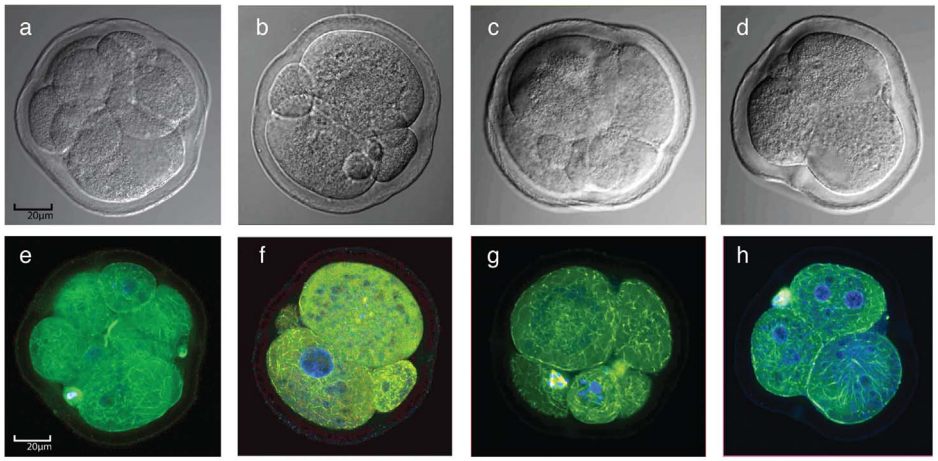

Figure 7 | Confocal brightfield (a–d) and fluorescence (e–h) micrographs of rhesus embryos resulting from ICSI fertilization with oxidatively stressed sperm. In each represented embryo, note extensive nuclear fragmentation and unequal blastomere size and integrity. Note abnormal mitotic figure in one embryo (g). Images were acquired using a 40×/NA 1.0 lens on an Olympus FV1000 Spectral Scan point scanning confocal running Olympus FluoView version 2.1 software. Noise in individual optical sections was reduced by summing multiple scans of each image (''Kalman filtering''). Differential Interference Contrast (DIC) images were recorded using unabsorbed excitation light at 488 nm. Three dimensional images were recorded after acquiring z-stack images of 1.62 um per sequential focal slice. Bar = 20µ.

Embryo development and sperm-based oxidative stress. In our study with embryos produced using in vitro oxidatively-stressed sperm, we report a higher increase of direct cleavage to three or more blastomeres at first cleavage. Confocal fluorescence imaging demonstrated profound abnormal nuclear events. All of the embryos fertilized by oxidatively-stressed sperm exhibited a Type 1 abnormal cleavage pattern and stopped cleaving by the third cell cycle. We cannot rule out that very rapid cell division seen in the P1 and P2 stages in this experiment was actually a type of fragmentation rather than true cleavage. Most stages of the cell cycle are simply too long for completion of a cell cycle in this time. It is similarly not clear which spermatozoal-based mechanism could result in disorganized early cleavage, or fragmentation, and micronucleation but sperm centrosomal contribution to the mitotic spindle could be a potential cause[44,45]. The complexities of centrosomal function in developing gametes and embryos have been elegantly reviewed and offer one possible mechanism for downstream effects from oxidatively damaged sperm[46,47]. It has been suggested that meiotic spindle centrosomes are highly susceptible to aging, drugs, or toxic agents[46] all of which are likely to have oxidative components. Further studies into the downstream effects of oxidative sperm insult are warranted in order to determine how paternal affects are imparted to mammalian embryos during post-fertilization development.

Although ICSI itself has been associated with abnormal cell cycle events in rhesus monkeys[48,49], the nuclear changes we have observed suggest an apoptotic mechanism for cell and nuclear fragmentation that could be induced by an excessive sperm oxidative state. The occurrence of the Type I abnormal cleavage pattern has been considered "sperm-driven" due to polyspermy[13,42,50], however, all of our embryos are ICSI-produced and polyspermy is not a factor in demise of these embryos. The production of Type 1 abnormalities were also observed with ICSI of single sperm heads injected into pig oocytes, therefore origin of this defect is still unknown[13]. The presence of micronuclei seen in these embryos could be due to daughter cells that subsequently exit mitosis due to abnormal chromosome complements thus preventing participation in mitosis followed by a combination of necrotic and apoptotic cell death[50].

Conclusion

In conclusion, our study has revealed parameters of cleavage and early cell division for embryos of a relevant animal model, the rhesus macaque, using a time-lapse imaging system that documents mitotic activity on a minute-to-minute basis. Using this tool, we have shown that oxidative stress to sperm can result in abnormal early developmental anomalies that lead to embryonic and fetal demise in this animal model for human development. This finding has implications for numerous conditions of inherited disease, diet, fertility, ozone and environmental effects, cancer, and childhood diseases-all of which exhibit degrees of the common denominator of oxidative cellular stress. The mechanisms of oxidative stress on organismal, cellular, and subcellular levels are not clearly defined and are likely multifactorial. Further studies are necessary to understand how oxidative stress is related to the cell arrest observed in these embryos.

1. Vanneste, E. *et al.* Chromosome instability is common in human cleavage-stage embryos. *Nat Med* **15**, 577–83 (2009).
2. Vanneste, E. *et al.* What next for preimplantation genetic screening? High mitotic chromosome instability rate provides the biological basis for the low success rate. *Hum Reprod* **24**, 2679–82 (2009).
3. Chavez, S. L. *et al.* Dynamic blastomere behaviour reflects human embryo ploidy by the four-cell stage. *Nat Commun* **3**, 1251 (2012).
4. Chen, A. A., Tan, L., Suraj, V., Reijo Pera, R. & Shen, S. Biomarkers identified with time-lapse imaging: discovery, validation, and practical application. *Fertil Steril* **99**, 1035–43 (2013).
5. Conaghan, J. *et al.* Improving embryo selection using a computer-automated time-lapse image analysis test plus day 3 morphology: results from a prospective multicenter trial. *Fertil Steril* **100**, 412–9 (2013).
6. Meseguer, M. *et al.* The use of morphokinetics as a predictor of embryo implantation. *Hum Reprod* **26**, 2658–71 (2011).
7. Wong, C., Chen, A. A., Behr, B. & Shen, S. Time-lapse microscopy and image analysis in basic and clinical embryo development research. *Reprod Biomed Online* **26**, 120–9 (2013).
8. Wirka, K. *et al.* Abnormal syngamy phenotypes observed with time-lapse imaging may allow early identification of embryos with lower development potential. *Hum. Reprod.* **28**, 188 (Abst) (2013).
9. Campbell, A. *et al.* Modelling a risk classification of aneuploidy in human embryos using non-invasive morphokinetics. *Reprod Biomed Online* **26**, 477–85 (2013).
10. Campbell, A. *et al.* Retrospective analysis of outcomes after IVF using an aneuploidy risk model derived from time-lapse imaging without PGS. *Reprod Biomed Online* **27**, 140–6 (2013).
11. Dal Canto, M. *et al.* Cleavage kinetics analysis of human embryos predicts development to blastocyst and implantation. *Reprod Biomed Online* **25**, 474–80 (2012).
12. Sandalinas, M. *et al.* Developmental ability of chromosomally abnormal human embryos to develop to the blastocyst stage. *Hum Reprod* **16**, 1954–8 (2001).
13. Somfai, T. *et al.* Relationship between the length of cell cycles, cleavage pattern and developmental competence in bovine embryos generated by in vitro fertilization or parthenogenesis. *J Reprod Dev* **56**, 200–7 (2010).

14. Janny, L. & Menezo, Y. J. Maternal age effect on early human embryonic development and blastocyst formation. *Mol Reprod Dev* **45**, 31–7 (1996).
15. Burruel, V., Klooster, K. L., Chitwood, J., Ross, P. J. & Meyers, S. A. Oxidative damage to rhesus macaque spermatozoa results in mitotic arrest and transcript abundance changes in early embryos. *Biol Reprod* **89**, 72 (2013).
16. Sarason, R. L., VandeVoort, C. A., Mader, D. R. & Overstreet, J. W. The use of nonmetal electrodes in electroejaculation of restrained but unanesthetized macaques. *J Med Primatol* **20**, 122–5 (1991).
17. Baumber, J. & Meyers, S. A. Changes in membrane lipid order with capacitation in rhesus macaque (Macaca mulatta) spermatozoa. *J Androl* **27**, 578–87 (2006).
18. Baumber, J. & Meyers, S. A. Hyperactivated motility in rhesus macaque (Macaca mulatta) spermatozoa. *J Androl* **27**, 459–68 (2006).
19. McCarthy, M. J., Baumber, J., Kass, P. H. & Meyers, S. A. Osmotic stress induces oxidative cell damage to rhesus macaque spermatozoa. *Biol Reprod* **82**, 644–51 (2010).
20. Organization, W.H. WHO laboratory manual for the examination and processing of human semen (Cambridge University Press, Cambridge, England, 2010).
21. Aitken, R. J., Buckingham, D. & Harkiss, D. Use of a xanthine oxidase free radical generating system to investigate the cytotoxic effects of reactive oxygen species on human spermatozoa. *J Reprod Fertil* **97**, 441–50 (1993).
22. McCord, J. M. & Fridovich, I. The reduction of cytochrome c by milk xanthine oxidase. *J Biol Chem* **243**, 5753–60 (1968).
23. Wolf, D. P. Assisted reproductive technologies in rhesus macaques. *Reprod Biol Endocrinol* **2**, 37 (2004).
24. Wolf, D. P. *et al.* Use of assisted reproductive technologies in the propagation of rhesus macaque offspring. *Biol Reprod* **71**, 486–93 (2004).
25. Meyers, S. A., Li, M. W., Enders, A. C. & Overstreet, J. W. Rhesus macaque blastocysts resulting from intracytoplasmic sperm injection of vacuum-dried spermatozoa. *J Med Primatol* **38**, 310–7 (2009).
26. Gardner, D. K. & Schoolcraft, W. B. in Towards reproductive certainty: fertility and genetics beyond 1999. (ed. Jansen, R. & Mortimer, D.) 378–388. (Parthenon Publishing, London, 1999).
27. Gardner, D. K. & Schoolcraft, W. B. A randomized trial of blastocyst culture and transfer in in-vitro fertilization: reply. *Hum Reprod* **14**, 1663A–1663 (1999).
28. Gardner, D. K. & Schoolcraft, W. B. Culture and transfer of human blastocysts. *Curr Opin Obstet Gynecol* **11**, 307–11 (1999).
29. Gvakharia, M. *et al.* Using a novel time-lapse platform with automated image analysis can detect diverse abnormal cleavage patterns that are not recognized by traditional morphology and correlate with poor implantation. *Fertil Steril* **100**, S463. Abstract (2013).
30. Klooster, K. L., Burruel, V. R. & Meyers, S. A. Loss of fertilization potential of desiccated rhesus macaque spermatozoa following prolonged storage. *Cryobiology* **62**, 161–6 (2011).
31. Mitalipov, S. M., Yeoman, R. R., Kuo, H. C. & Wolf, D. P. Monozygotic twinning in rhesus monkeys by manipulation of in vitro-derived embryos. *Biol Reprod* **66**, 1449–55 (2002).
32. Yeoman, R. R. *et al.* Cryoloop vitrification yields superior survival of Rhesus monkey blastocysts. *Hum Reprod* **16**, 1965–9 (2001).
33. Goodeaux, L. *et al.* Successful nonsurgical collection of Macaca mulatta embryos. *Theriogenology* **34**, 1159–1167. (1990).
34. Magli, M. C. *et al.* Embryo morphology and development are dependent on the chromosomal complement. *Fertil Steril* **87**, 534–41 (2007).
35. Dupont, C. *et al.* Incidence of chromosomal mosaicism in morphologically normal nonhuman primate preimplantation embryos. *Fertil Steril* **93**, 2545–50 (2010).
36. Bielanska, M., Tan, S. L. & Ao, A. Different probe combinations for assessment of postzygotic chromosomal imbalances in human embryos. *J Assist Reprod Genet* **19**, 177–82 (2002).
37. Biggers, J. D. & Racowsky, C. The development of fertilized human ova to the blastocyst stage in KSOM(AA) medium: is a two-step protocol necessary? *Reprod Biomed Online* **5**, 133–40 (2002).
38. Weston, A. M. & Wolf, D. P. Differential preimplantation development of rhesus monkey embryos in serum-supplemented media. *Mol Reprod Dev* **44**, 88–92 (1996).
39. Wiemer, K. E., Anderson, A. R., Kyslinger, M. L. & Weikert, M. L. Embryonic development and pregnancies following sequential culture in human tubal fluid and a modified simplex optimized medium containing amino acids. *Reprod Biomed Online* **5**, 323–7 (2002).
40. Conaghan, J. *et al.* Embryos exhibiting abnormal first cytokinesis phenotypes are associated with poorer embryo development and lower implantation potential. *Fertil Steril* **100**, S90 (2013).
41. Alikani, M. *et al.* Cleavage anomalies in early human embryos and survival after prolonged culture in-vitro. *Hum Reprod* **15**, 2634–43 (2000).
42. Sugimura, S. *et al.* Promising system for selecting healthy in vitro-fertilized embryos in cattle. *PLoS One* **7**, e36627 (2012).
43. Simerly, C. & Schatten, G. Chapter 4, Utility of Animal Models for Human Embryo Culture; Nonhuman Primates (Springer Science + Business Media, LLC 2012).
44. Hewitson, L. C. *et al.* Microtubule and chromatin configurations during rhesus intracytoplasmic sperm injection: successes and failures. *Biol Reprod* **55**, 271–80 (1996).
45. Sutovsky, P. *et al.* Intracytoplasmic sperm injection for Rhesus monkey fertilization results in unusual chromatin, cytoskeletal, and membrane events, but eventually leads to pronuclear development and sperm aster assembly. *Hum Reprod* **11**, 1703–12 (1996).
46. Schatten, H. & Sun, Q. Y. The functional significance of centrosomes in mammalian meiosis, fertilization, development, nuclear transfer, and stem cell differentiation. *Environ Mol Mutagen* **50**, 620–36 (2009).
47. Schatten, H. & Sun, Q. Y. The role of centrosomes in fertilization, cell division and establishment of asymmetry during embryo development. *Semin Cell Dev Biol* **21**, 174–84 (2010).
48. Hewitson, L. *et al.* Unique checkpoints during the first cell cycle of fertilization after intracytoplasmic sperm injection in rhesus monkeys. *Nat Med* **5**, 431–3 (1999).
49. Hewitson, L., Martinovich, C., Simerly, C., Takahashi, D. & Schatten, G. Rhesus offspring produced by intracytoplasmic injection of testicular sperm and elongated spermatids. *Fertil Steril* **77**, 794–801 (2002).
50. Chatzimeletiou, K., Morrison, E. E., Prapas, N., Prapas, Y. & Handyside, A. H. Spindle abnormalities in normally developing and arrested human preimplantation embryos in vitro identified by confocal laser scanning microscopy. *Hum Reprod* **20**, 672–82 (2005).

Acknowledgments

We gratefully acknowledge Merck, Inc (Whitehouse Station, NJ) for generous donation of recombinant human gonadotropins for superovulation of rhesus females in this study. The authors wish to thank Dr. Shawn Chavez, Oregon Health Sciences University, for assistance with analysis and interpretation of non-invasive embryo imaging data. We gratefully thank, Dr. Alice Chen, Auxogyn, Inc, (Menlo Park, CA) for technical assistance and generous donation of the darkfield Early Embryo Viability Assessment (EEVA) system and software. We also thank Tawny Scanlan and Kathy West for schematic embryo drawings. Stephen Bennett for figures, and Dr. Michael Paddy, Department of Molecular and Cellular Biology, UC Davis, for confocal fluorescence imaging and analysis.

Author contributions

V.B. coordinated and performed all experiments with oocytes and embryo culture and was primary author. K.K. performed all spermatozoal treatments and edited the manuscript. C.B. performed statistical analysis and contributed to the manuscript. R.R.P. contributed to experimental design and manuscript editing. S.M. designed all experiments, supervised all animal studies, and co-wrote the manuscript with V.B.

Additional information

Competing financial interests: The authors declare no competing financial interests.

How to cite this article: Burruel, V., Klooster, K., Barker, C.M., Pera, R.R. & Meyers, S. Abnormal Early Cleavage Events Predict Early Embryo Demise: Sperm Oxidative Stress and Early Abnormal Cleavage. *Sci. Rep.* **4**, 6598; DOI:10.1038/srep06598 (2014).